Optically tuned and large-grained bromine doped $CH_3NH_3PbI_3$ perovskite thin films via aerosol-assisted chemical vapour deposition

Shreya Basak,[a] Mohammad Afzaal,*[b,¶] and Heather M. Yates,[b]

[a]Department of Physical Sciences, Indian Institute of Science Education and Research Kolkata, Mohanpur, 741246, West Bengal, India

[b]Materials and Physics Research Centre, University of Salford, Salford, M5 4WT, United Kingdom. E-mail: moh.afzaal@gmail.com

[¶]Current Address: Math & Natural Science Division, Higher Colleges of Technology, P.O.Box: 7947, Sharjah, United Arab Emirates

Abstract:

Herein, doping of methylammonium lead iodide perovskite thin films with bromine ions is successfully performed for the first time using the aerosol-assisted chemical vapour deposition process. Depending on the doping levels, photoluminescence spectra are shifted relative to their bandgap values. Detailed analysis of scanning electron microscope images showed that increasing the bromine levels linearly increased the grain sizes. The unchanged amount of detected lead provided evidence for the controlled processing conditions. Both bulk and surface compositional techniques confirmed the deposition of marginally iodine rich perovskite thin films.

1. Introduction

A quest to deliver inexpensive and efficient solar cells has spurred a worldwide response into perovskite (PK) photovoltaic technologies, which have attributed to power conversion efficiency (PCEs) values in excess of 20% for prototype devices [1]. Interest in PK solar cells is driven by the exceptional optoelectronic characteristics of the absorber layers, in particular large carrier diffusion lengths, suitable bandgaps and small exciton binding energies [2-6]. Other important factors include low processing costs, abundant raw materials and less capital-intensive manufacturing processes.

For highly efficient PK solar cells, spin-coating is often the preferred choice of technique for depositing PK absorbers [7]. Despite the enormous progress made on various technological facets [8-10], production of large area PK coatings with enhanced stabilities is still challenging. For cost-effective and large area deposition of PK coatings, chemical vapour deposition (CVD) processes provide a highly attractive way to meet increasing demand [11-13]. Various modifications of CVD processes are available, such as atmospheric-pressure (AP) CVD [11] which is suited for achieving continuous and faster growth rates and can be added to in-line processes, for example, float glass lines. On the contrary, low-pressure processes require high capital equipment and process costs, and often need precursors with high vapour pressures [12].

A solution-based technique aerosol-assisted (AA) CVD is an attractive option for depositing coatings at atmospheric pressure conditions [14]. The process obviates the need for high vapour pressure metal alkyl precursors and relies on the solubility of low-cost precursors in common organic solvents. From an industrial scale point of view, it is also feasible to transfer precursor aerosol mist to existing processing lines. Various groups including ours have adopted the technique for one-step deposition of $CH_3NH_3PbI_3$ thin films [15-17]. However, the resulting films were generally non-uniform, composed of aggregates of particles and had poor coverage. We attribute the observed morphologies to be a result of early gas phase nucleation between the precursors before reaching the heated substrates. For increased stability and optical tunability mixed halide PK layers have been reported and analysed in PV devices [18-20]. Doping of $CH_3NH_3PbI_3$ thin films with bromine is a viable way of increasing the perovskite stability, enhance carrier transport and band gap tuning. For the first time, we employed the AACVD process for the successful doping of PK thin films and probe how optical and structural properties respond to different doping levels. The different levels of bromine will alter both conduction and valence band positions, allowing a

range of wider energy bands which, in turn, provide larger open circuit voltages in the solar cells [3,21]. The over-riding reason for use of this AACVD process is its simplicity, as it allows simple mixing of multiple precursors in same solvent (in same flask) and straightforward rendition of the precursor delivery, with the aid of a carrier gas.

2. Experimental details

Prior to any deposition experiments, 1.1 mm borosilicate glass (Corning Eagle 2000) substrates were cleaned with detergent, water, propan-2-ol, and dried in air. Vicks pediatric mini ultrasonic humidifier was used as the nebulizer. Methylammonium iodide (CH_3NH_3I) was purchased from Solaronix. Lead iodide (PbI_2), lead bromide ($PbBr_2$) and dimethylformamide (DMF) acquired from Sigma Aldrich Ltd were used as received. A Platon NGX glass variable area flowmeter was used to control the N_2 flow.

2.1. Deposition of Thin films

The AACVD experimental set-up and procedure was similar to that described in a previous report [22]. The system was purged for 1 hr under a constant flow rate of N_2 (0.5L/min) at 140 °C prior to deposition experiments. After stirring controlled amounts of PbI_2 (1.533 – 0 mmol), $PbBr_2$ (0 – 1.533 mmol) and CH_3NH_3I (4.61 mmol) in 6 ml DMF under N_2 for 1 hr, resulting transparent yellow solutions were utilised for the deposition of thin films. The substrates were heated at 140 °C using a standard electric furnace with a constant N_2 supply of 0.5L/min. After 45 mins of deposition time, films were quickly removed and transferred to a glove box.

1.2. Characterisation of thin films

Transmission and reflection measurement were performed on an Aquila nkd 8000 spectrophotometer between 350 - 1000 nm at an incident angle of 30° using p polarization. The Eg was calculated from a Tauc plot of $(\alpha h\nu)^2$ versus energy where α is the absorption coefficient (derived from $\alpha = -\ln[T/(1-R)]/t$ where T = transmission, R = reflection and t = film thickness) and $h\nu$ is the photon energy [23]. Scanning electron microscope images were recorded on a Philips XL-30 FEG SEM. Using ImageJ [24], resulting SEM images were analyzed to determine particle sizes. Photoluminescence measurements used an excitation wavelength of 405 nm and an experimental set-up as described previously [25]. X-ray photoelectron spectroscopy (XPS) was performed on a Thermo Fisher Scientific NEXSA spectrometer. For the XPS studies, samples were packed and sealed in the glovebox, before being vacuum packed for transport. Samples were analysed using a micro-focused monochromatic Al X-ray source (72 W) over an area of approximately 400 microns. Data was

recorded at pass energies of 200 eV for survey scans and 50 eV for high resolution scan with 1 eV and 0.1 eV step sizes respectively. Charge neutralisation of the sample was achieved using a combination of both low energy electrons and argon ions. Scans were performed both before and after sample etching to remove any surface contaminants. The etching was conducted by argon sputtering for 10 s with a beam voltage of 1 kV, spot size of 2 x 2 mm^2 and sputter rate (Ta_2O_5) = 0.26 nm/s. Data analysis was performed in CasaXPS using a Shirley type background and Scofield cross sections, with an energy dependence of -0.6. X-ray powder diffraction measurements were carried out using a Siemen D5000 instrument. Crystallite size was calculated by Scherrer equation.

$$D = \frac{0.94\lambda}{\beta\cos\theta}$$

3. Results and Discussion

Controlled amounts of PbI_2 and $PbBr_2$ were added to a stirring solution of CH_3NH_3I in DMF N_2. After 1 hr, the flask was connected to a precursor delivery tube with N_2 carrier gas, growth time and deposition temperature fixed at 0.5 l/min, 45 mins and 140 (± 2) °C, respectively. Immediately after the deposition, the samples were transferred from the open laboratory to a dry glovebox and stored. Depending on the $PbBr_2$:PbI_2 ratio within the flask, films with a range of colours were deposited as shown on Fig. 1. The ratio, *y*, is defined as the $PbBr_2$ concentration relative to the total lead halide concentration. Deposited films were found to be uniform and adherent, although their surface could be scratched by a scalpel.

Fig. 1. A photo of segments of resulting perovskite thin films with increased bromine levels (from left to right).

The X-ray powder diffraction (XRD) studies confirmed the films to be predominantly composed of room temperature stable tetragonal $CH_3NH_3PbI_3$ (*I4/mcm*) phase with a preferred orientation along the (220) plane, although a minor $(CH_3NH_3)_4PbI_6.2H_2O$ component was also evident (Fig. 2 top). Increasing the Br^- ion concentration marginally shifted the (220) peak

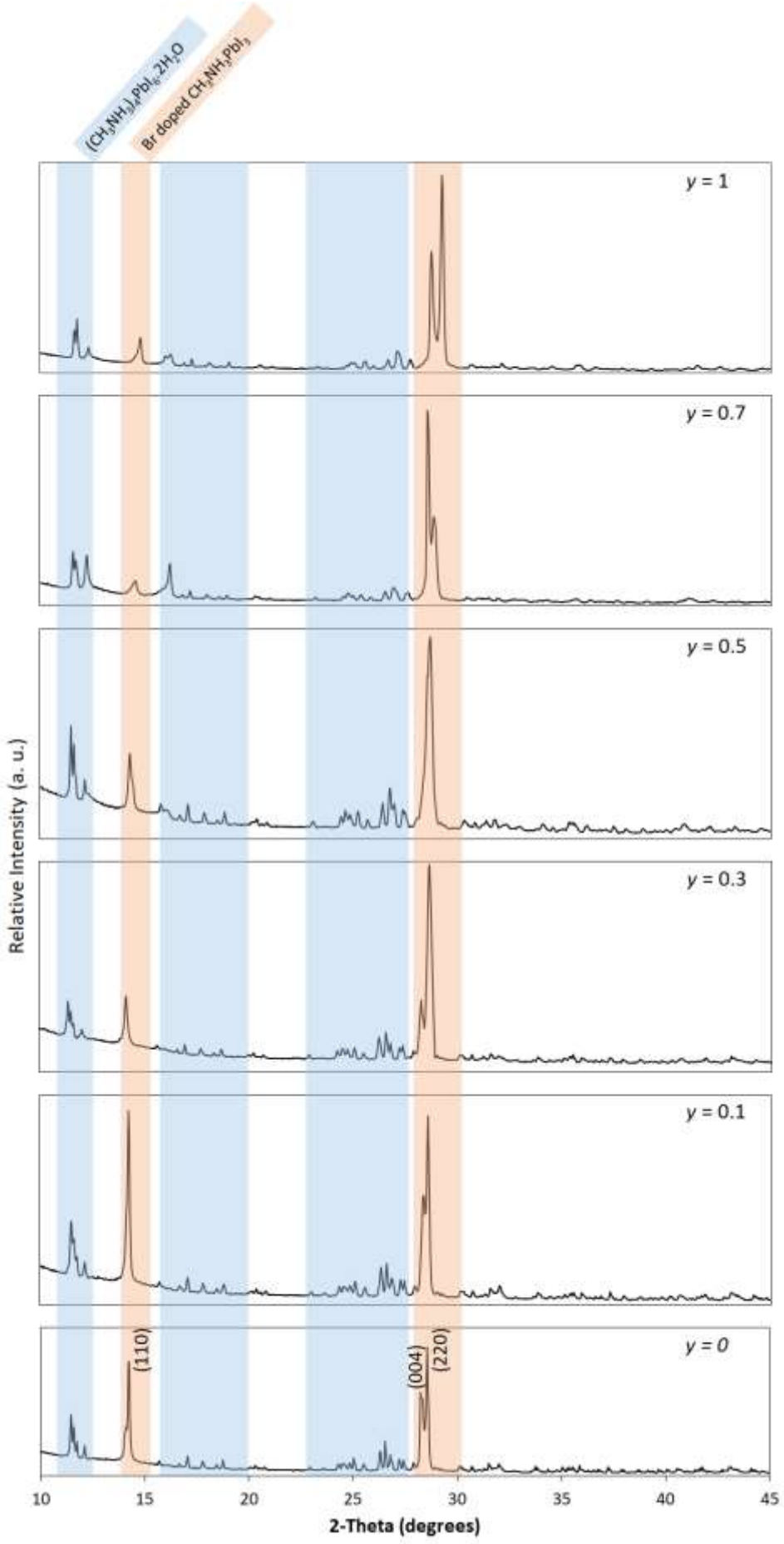
(CH3NH3)4PbI6·2H2O
Br doped CH3NH3PbI3
y = 1
y = 0.7
y = 0.5
y = 0.3
y = 0.1
y = 0
(110)
(004)
(220)
Relative Intensity (a. u.)
10
15
20
25
30
35
40
45
2-Theta (degrees)

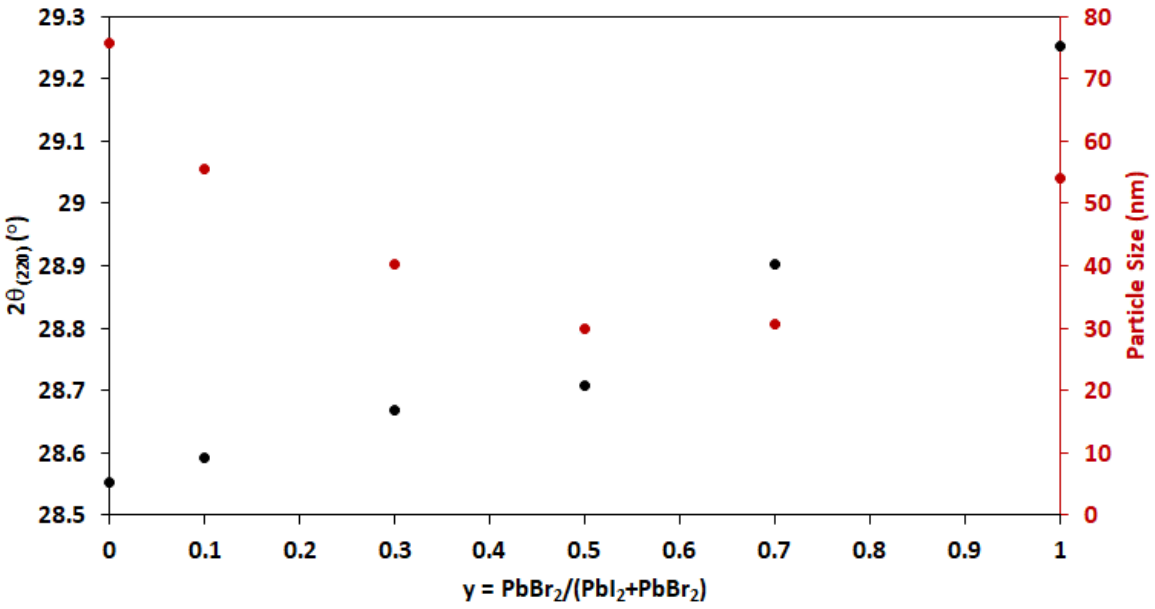

Fig. 2. (Top) XRD patterns of $CH_3NH_3Pb(I_{1-x}Br_x)_3$ thin films. (Bottom) The (220) peak positions and particle sizes for $CH_3NH_3Pb(I_{1-x}Br_x)_3$ thin films.

towards higher angles indicating a contraction in lattice parameter as larger I^- (2.2Å) were easily substituted with smaller Br^- (1.9Å) ions [26]. (Figure 2 bottom). At $y = 0.5$, the resulting XRD shift caused the (004) peak to overlap its neighbouring (220) peak and hence, it is absent in our XRD pattern. There was no evidence of any starting materials in the resulting diffraction patterns. From the Scherrer equation, difference in particle sizes could be traced to the changes in full width at half maximum which correspond to local strain and local variations of bromine ions throughout the lattice as previously suggested (Fig. 2 bottom) [27]. We strongly suspect the detection of dihydrate to be a result of high relative humidity (RH) of the laboratory as shown by the thermo-hygrometer readings (RH = 75 % at 21 °C). This observation supports a previous study where at high RH of 80%, $CH_3NH_3PbI_3$ converted to dehydrate species [28]. It is noted that the monohydrate species were also formed in the presence of moisture [26] which after comparing the diffraction data with monohydrate crystals, are absent in the present work.

Scanning electron microscope (SEM) studies showed the formation of continuous, dense and (almost) pinhole free films. The present study is in sharp contrast to previous one-step AACVD attempts where non-homogenous PK films were attempted [15-17]. Interestingly after analysing the images, a trend emerges where the grain size increase linearly with increasing the amount of $PbBr_2$ in the mother solution (Figure 3). Depending on the precursor ratios, average grain sizes beyond 1 μm could be obtained which in turn implies reduced grain boundaries ideal for efficient charge transportation of charges in PK solar cells. Bulk energy dispersive X-ray analysis (EDX) showed that the bromine levels increased linearly with increasing $PbBr_2$ precursor, with a concomitant decrease in the iodine content, as expected (Figure S1). One common trend in the all the films was the presence of excess halide. (Table S1) As the resulting atomic percentage of lead was found to be consistent in the films, it reflects the control over the growth process and the ability to give precisely doped films.

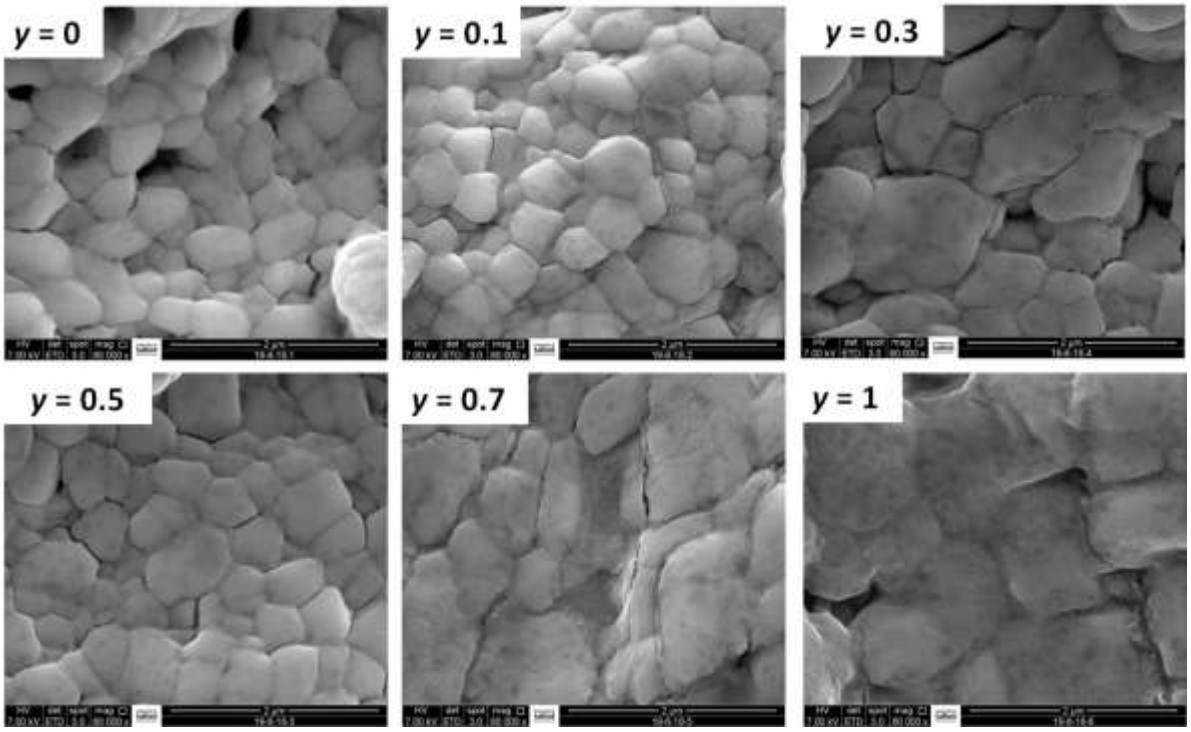

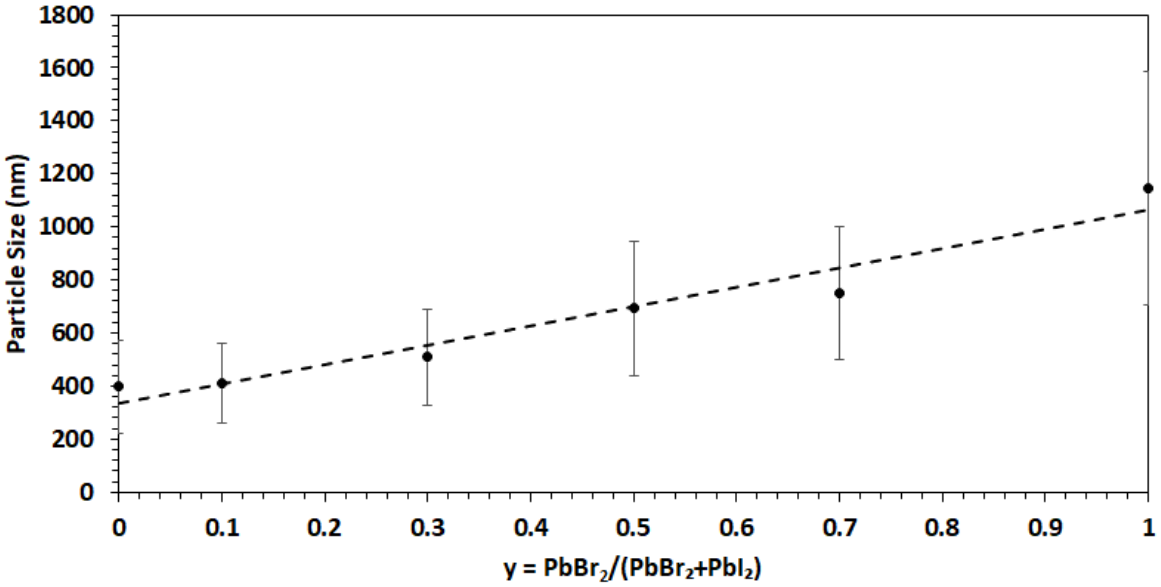

Fig. 3. (Top) SEM images and (bottom) ImageJ analysis of $CH_3NH_3Pb(I_{1-x}Br_x)_3$ thin films. Scale = 2 μm

From the Tauc plots, the effects of bromine levels on the optical bandgaps of PK films were tracked. By extrapolating the linear regions to the *x* intercept, it became clear that the bandgaps continuously blue-shifted from 1.48 to 2.0 eV with increased bromine levels in the solution and hence sample (Figure 4 top). Similarly, after exciting the films with a blue laser and recording their photoemission, their maximum values blue-shifted from 771 nm (1.61 eV) to 684 nm (1.81 eV) nm. Our bromine dependent optical characteristics are consistent with other spin coated mixed halide PK thin films [19]. A minor broad peak at higher wavelengths is attributed to second-order emission of the blue laser. This was confirmed by running the analysis with a blank substrate. Depending on the Br^- levels, photoluminescence (PL) spectra were either blue- or red-shifted relative to their absorption edges as evident in Figure 4. To illustrate the point, the PL spectra is marginally blue-shifted (i.e. anti-Stokes shift) with respect its absorption edge for samples with low doping levels ($y = 0 - 0.3$). Such type of behavior in PKs is proposed to be a result of number of factors including coulomb interaction, vibration relaxation, exciton binding energy [29,30]. On the contrary, samples with $y \geq 0.5$, the maximum positions of PL signals are strongly shifted to the red (Stokes shift) compared with respect to their bandgaps. This is caused by a large self-absorption ratio of PK films and is considered advantageous from the point of view of efficient photon recycling because it leads to enhance solar cell efficiencies [31]. Due to the absence of PL data in previous AACVD studies [15-17], a direct comparison between the resulting optical properties cannot be made.

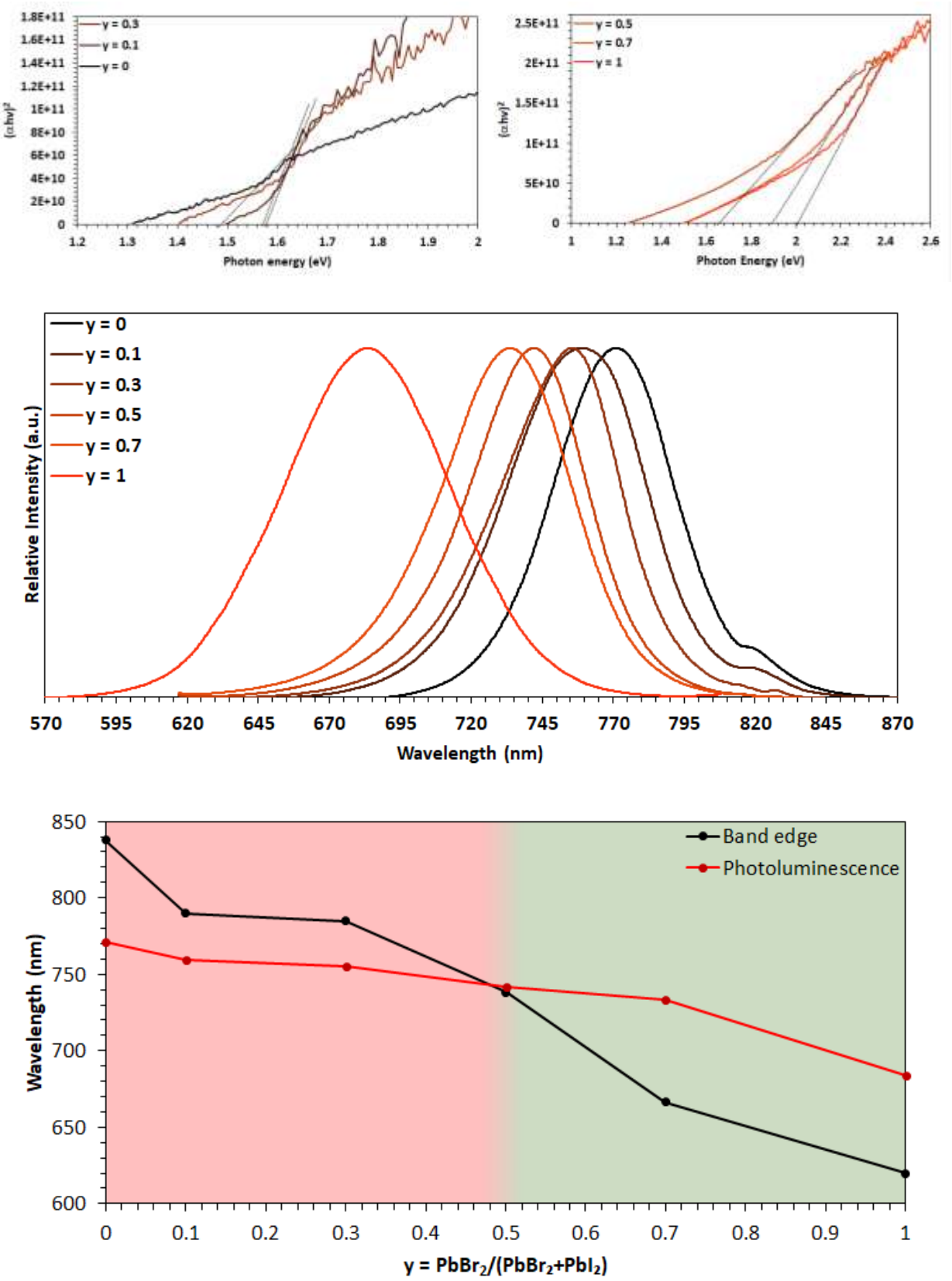

Fig. 4 (Top) Tauc plots, (middle) photoluminescence spectra and (bottom) resulting wavelengths for $CH_3NH_3Pb(I_{1-x}Br_x)_3$ thin films.

The EDX gives the average bulk distribution of the elements present in the films and was used to determine the relative elemental ratios. However, this cannot give any information on the chemical state of the element nor whether it is a surface contaminant or bulk film. In addition, EDX is unable to detect N with any accuracy. To understand the surface chemistry of the films better it was necessary to use X-ray photoelectron spectroscopy (XPS). The survey scan of all 6 samples established the presence of Pb, I, N and C. The samples with the highest Br concentrations (y = 0.7, 1.0) also showed a very small O signal at 533.2 eV generally assigned to absorbed water. The intensity of this reduced after a 10 sec argon etch, confirming it related to surface contamination. Despite the direct evidence from EDX and indirect from optical and structural measurements there is only a very small signal for Br evident in the wide scan for y = 0.5 to 1.0. This even at its greatest intensity (in y = 1) was too small to accurately determine its relative concentration (~ 7%). The same sample under EDX gave a value of 36%. The disparity in the relative concentration of Br between the two techniques can be accounted for by two main reasons. Firstly, XPS only probes the top few nanometers of a surface while EDX probes to a much greater depth. The difference between surface and bulk could relate to some surface degradation due to the time between deposition of the film and analysis, with preferential removal of the Br. For EDX the films were analyzed within a few hours of deposition, while for XPS it was a few weeks. As previously reported by Wang et al. [32] PK gradually degrades in air due to absorption of moisture and oxidation of the halide and its subsequent release from the sample. This was curtailed by storage of the samples in a dry glovebox and by sealing the samples in evacuated bags for transport. As the O 1s signal is extremely weak to non-existent, the amount of moisture absorbed and hence degradation by this route was minimal. Hence the discrepancy is more likely to relate to the sensitivity of XPS to detect Br. This is determined by both the number of electrons leaving a sample surface and the efficiency of the instrument to detect the emitted photoelectrons at specific energies. For quantitative analysis, Relative Sensitivity Factors (RSF) are used to scale the measured peak areas so they are representative of the amount of material in the sample. In the case of Br they are very much smaller than those for I (RSF 2.84 to 33.64 for the 3d peaks) and increase the difficulty of obtaining good signal/noise and clearly defined peaks.

The C1s high resolution scans could be resolved into two signals a smaller one relating to amorphous C (285.2 eV) and a much stronger signal at 286.8 eV relating to the carbon within the methylammonium cation [33]. High resolution scans for N 1s showed a single peak at 402.7 eV, indicating that there is only one N species present and in good agreement with values reported previously for the quaternary ammonium cation (Figure S2) [34]. Similarly, I 3d only

showed a single chemical state with the $3d_{5/2}$ peak at 619.6 eV with a splitting of 11.5 eV (Figure S3) [35].

Although Br was not seen clearly in the survey scan it could be detected in the higher resolution scan and resolved into 2 peaks with the $3d_{5/2}$ 68.9 eV and a splitting of 1.05 eV characteristic of that for a Br ion [36]. Figure 5 clearly shows the increase in intensity and hence concentration of Br ion with increased precursor ratio, hence mirroring the EDX result.

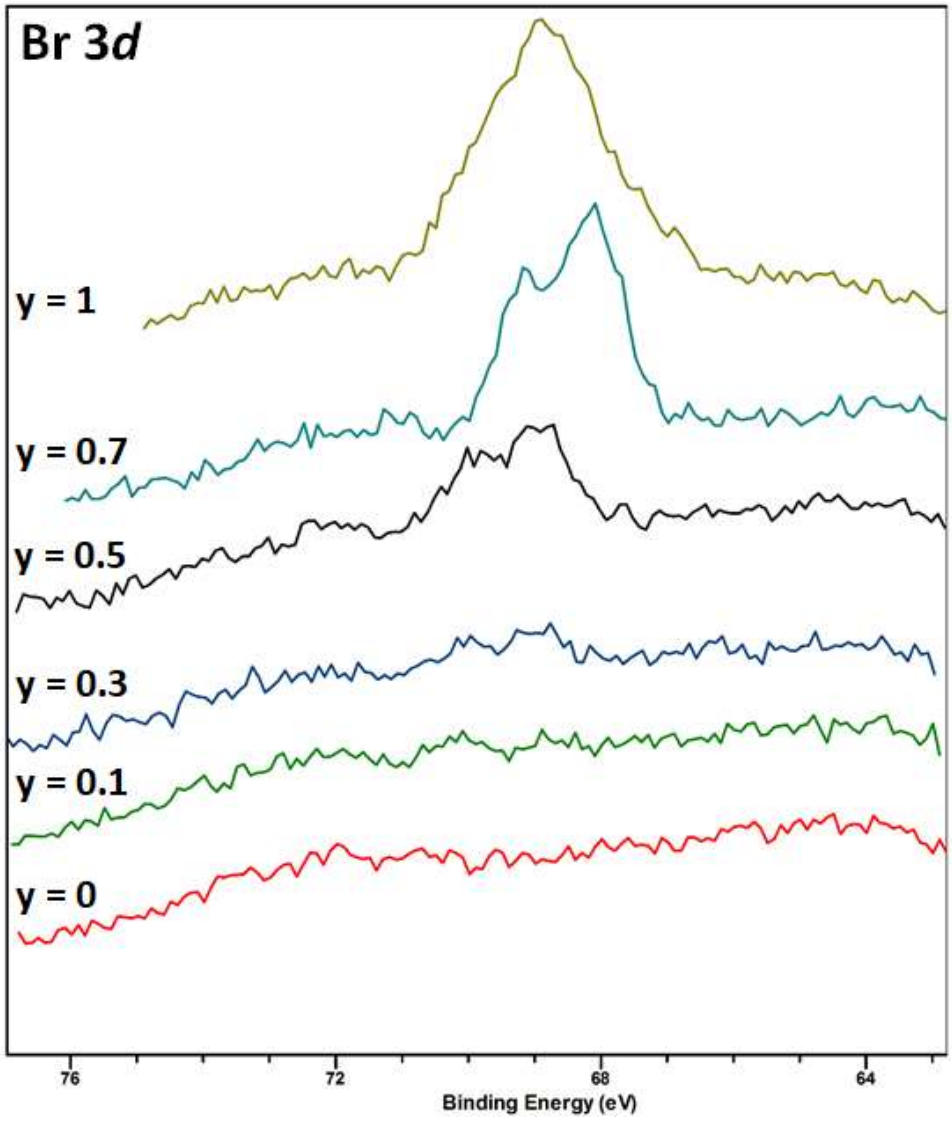

Fig. 5. High-resolution XPS spectra of the Br 3d region for $CH_3NH_3Pb(I_{1-x}Br_x)_3$ thin films.

In all samples, there is a strong Pb 4f doublet with the $4f_{7/2}$ at 138.7 eV and splitting of 4.85 eV in agreement with Pb within PK (Figure S4). In some samples, especially after the Ar etch there is the presence of a lower intensity shoulder fitted to 137.2 eV related to metallic Pb (7 ± 2) % and generally ascribed to laser irradiation [37] or beam damage during measurements [35]. As the BE for Pb attached to Br or I is extremely close (within 0.1eV) [38] it is impossible to

determine the proportion of Pb mainly attached to each halide. In addition it can been seen from both databases (NIST) and literature that there is only a shift of 0.3 eV between Pb $4f_{7/2}$ within PbI_2 and $MAPbI_3$ [39].

For determination of the stoichiometry, both the metallic Pb and amorphous C components (Figure S5) were removed prior to the calculation. As can be seen in table 1 the ratio of Pb:I:N:C is not that of a perfect PK samples (1:3:1:1). In general there is slightly too much iodide (especially when considering the 'missing' bromide) and carbon. The reduction in iodide for samples y = 0.7 and 1.0 could be due to them containing the highest level of bromide.

Table 1. Compositions of different components in deposited films determined from XPS

y = $PbBr_2$/$PbBr_2$+PbI_2	Pb	I	N	C
0	1	3.2	1.1	1.3
0.1	1	3.2	1.0	1.5
0.3	1	3.2	1.1	1.5
0.5	1	3.2	1.1	1.3
0.7	1	3.0	1.0	1.4
1.0	1	2.7	1.0	1.4

It is possible that the excess halide, together with the C (from the methylammonium cation) relates to excess MAI. The N 1s signal overlaps with that of the much stronger Pb $4d_{5/2}$ so its concentration may have been under estimated. Against this argument, it can be seen that none of the XRD spectra showed any sign of the precursors. Neither was there any sign of absorption edges or bandgaps seen for the Pb halides in the optical measurements. Unfortunately, as explained earlier it is not possible to distinguish between the potentially different halide structures by XPS.

4. Conclusion

In summary, we have successfully demonstrated for the first time that a solution-based AACVD process can be used to deposit good quality mixed-halide PK thin films directly on glass. Unaltered lead levels within the films reflects precise control over the growth and processing conditions. Depending on the dopant levels, photoluminescent peaks were either Stokes or Anti-Stokes shifted relative to their absorption peaks. Detailed compositional analysis revealed the growth of slightly iodine rich PK thin films.

Competing financial interests

The authors declare no competing financial interests.

Acknowledgements

This work has received funding from the European Union's Horizon 2020 research and innovation programme under grant agreement No. 653296 (CHEOPS). The authors thank Dr J. E. Proctor and H. Malik (University of Salford) for their help with the photoluminescence measurements. XPS data collection was performed at the EPSRC National Facility for XPS ('HarwellXPS'), operated by Cardiff University and UCL, under contract No. PR16195.

References

[1] https://www.nrel.gov/pv/assets/images/efficiency-chart.png.

[2] S. D. Stranks, H. J. Snaith, Metal-halide perovskites for photovoltaic and light-emitting devices. Nat. Nanotechnol. 10 (2015) 391-402.

[3] M. A. Green, A. Ho-Baillie, H. J. Snaith, The emergence of perovskite solar cells. Nat. Photonics 8 (2014) 506-514.

[4] M. Petrović, V. Chellappan, S. Ramakrishna, Perovskites: Solar cells & engineering applications - materials and device developments. Sol. Energy 122 (2015) 678-699.

[5] P. Gao, M. Gratzel, M. K. Nazeeruddin, Organohalide lead perovskites for photovoltaic applications. Energy Environ. Sci. 7 (2014), 2448-2463.

[6] P. Löper, M. Stuckelberger, B. Niesen, J. Werner, M. Filipic, S.-J. Moon, J.-H. Yum, M. Topic, S. De Wolf, C. Ballif, Complex Refractive Index Spectra of $CH_3NH_3PbI_3$ Perovskite Thin Films Determined by Spectroscopic Ellipsometry and Spectrophotometry. J. Phys. Chem. Lett. 6 (2015) 66–71.

[7] Asghar, M. I.; Zhang, J.; Wang, H.; Lund, P. D. Device stability of perovskite solar cells - A review. Renewable and Sustainable Energy Reviews 77 (2017) 131–146.

[8] N.-G. Park, M. Grätzel, T. Miyasaka, K. Zhu, K. Emery, K. Towards stable and commercially available perovskite solar cells. Nature Energy 1 (2016) 16152.

[9] M. A. Green, A. Ho-Baillie, A. Perovskite Solar Cells: The Birth of a New Era in Photovoltaics. ACS Energy Lett. 2 (2017) 822–830.

[10] Y. C. Chen, L. R. Zhang, Y. Z. Zhang, H. L. Gao, H. Yan, Large-area perovskite solar cells - a review of recent progress and issues. RSC Adv. 8 (2018) 10489-10508.

[11] M. R. Leyden, L. K. Ono, S. R. Raga, Y. Kato, S. H. Wang, Y. B. Qi, High performance perovskite solar cells by hybrid chemical vapor deposition. J. Mater. Chem. A 2 (2014) 18742-18745.

[12] P. F. Luo, Z. F. Liu, W. Xia, C.C. Yuan, J. G. Cheng, Y. W. Lu, Uniform, Stable, and Efficient Planar-Heterojunction Perovskite Solar Cells by Facile Low-Pressure Chemical Vapor Deposition under Fully Open-Air Conditions. ACS Appl. Mater. Interfaces 7 (2015) 2708–2714.

[13] Q. Chen, H. P. Zhou, Z. R. Hong, S. Luo, H.-S. Duan, H.-H. Wang, Y. S. Liu, G. Li, Y. Yang, J. Am. Chem. Soc. 136 (2014) 622–625.

[14] M. J. Powell, D. B. Potter, R. L. Wilson, J. A. Darr, I. P. Parkin, C. J. Carmalt, Scaling aerosol assisted chemical vapour deposition: Exploring the relationship between growth rate and film properties. Mater. Design 129 (2017) 116-124.

[15] M. Afzaal, H. M. Yates, Growth patterns and properties of aerosol-assisted chemical vapor deposition of $CH_3NH_3PbI_3$ films in a single step. Surf. Coat. Tech. 321 (2017) 336-340.

[16] D. S. Bhachu, D. O.Scanlon, E. J. Saban, H. Bronstein, I. P. Parkin, C. J. Carmalt, R. G. Palgrave, Scalable route to $CH_3NH_3PbI_3$ perovskite thin films by aerosol assisted chemical vapour deposition, J. Mater. Chem. A 3 (2015) 9071-9073.

[17] D. J. Lewis, P. O'Brien, Ambient pressure aerosol-assisted chemical vapour deposition of $(CH_3NH_3)PbBr_3$, an inorganic-organic perovskite important in photovoltaics. Chem. Commun. 50 (2014) 6319-6321.

[18] M. J. Yang, et al. Facile fabrication of large-grain $CH_3NH_3PbI_{3-x}Br_x$ films for high-efficiency solar cells via CH_3NH_3Br-selective Ostwald ripening. Nat. Commun. 7 (2016) 12305.

[19] L. Q. Phuong, I. L. Braly, J. K. Katahara, H. W. Hillhouse, Y. Kanemitsu, Nonlinear photocarrier recombination dynamics in mixed-halide $CH_3NH_3Pb(I_{1-x}Br_x)_3$ perovskite thin films. Appl. Phys. Express 10 (2017)102401.

[20] S. Pont, D. Bryant, C.-T. Lin, N. Aristidou, S. Wheeler, X. R. Ma, R. Godin, S. A. Haque J. R. Durrant, Tuning $CH_3NH_3Pb(I_{1-x}Br_x)_3$ perovskite oxygen stability in thin films and solar cells. J. Mater. Chem. A 5 (2017) 9553-9560.

[21] (a) W. S. Yang, J. H. Noh, N. J. Jeon, Y. C. Kim, S. Ryu, J. Seo, S. I. Seok, High-performance photovoltaic perovskite layers fabricated through intramolecular exchange. Science 348 (2015) 1234–1237; (b) C. M. Sutter-Fella, Y. B. Li, M. Amani, J. W. Ager, F. M. Toma, E. Yablonovitch, I. D. Sharp, A. Javey, High Photoluminescence Quantum Yield in Band Gap Tunable Bromide Containing Mixed Halide Perovskites. Nano Lett. 16 (2016) 800–806; (c) B. Murali, et al. Surface Restructuring of Hybrid Perovskite Crystals. ACS Energy Lett. 1 (2016) 1119–1126.

[22] G. A. Horley, M. R. Lazell, P. O'Brien, Deposition of thin films of gallium sulfide from a novel liquid single-source precursor, $Ga(SOCNEt_2)_3$, by aerosol-assisted CVD, Chem. Vap. Deposition 5 (1999) 203-205.

[23] E. T. Hoke, D. J. Slotcavage, E. R. Dohner, A. R.; Bowring, H. I. Karunadasa, M. D. McGehee, Reversible photo-induced trap formation in mixed halide hybrid perovskites for photovoltaics, Chem. Sci. 6 (2015) 613-617.

[24] https://imagej.nih.gov/ij/download.html

[25] D. Smith, R. T. Howie, I. F. Crowe, C. L. Simionescu, C. Muryn, V. Vishnyakov, K.S. Novoselov, Y.-J. Kim, M. P. Halsall, E. Gregoryanz, J. E. Proctor, Hydrogenation of graphene by reaction at high pressure and high temperature, ACS Nano 9 (2015) 8279-8283.

[26] X. Guo, C. McCleese, C. Kolodziej, A. C. S. Samia, Y. X. Zhao, C. Burda, Identification and characterization of the intermediate phase in hybrid organic–inorganic $MAPbI_3$ perovskite. Dalton Trans. 45 (2016) 3806-3813.

[27] C. G. Bischak, C. L. Hetherington, H. Wu, S. Aloni, D. F. Ogletree, D. T. Limmer, N. S. Ginsberg, Origin of reversible photoinduced phase separation in hybrid perovskites. Nano Lett. 17 (2017) 1028–1033.

[28] A. M. A. Leguy, et al. Reversible hydration of $CH_3NH_3PbI_3$ in films, single crystals, and solar cells. Chem. Mater. 27 (2015) 3397–3407.

[29] C. M. Sutter-Fella, Q. P. Ngo, N. Cefarin, K. L. Gardner, N. Tamura, C. V. Stan, W. S. Drisdell, A. Javey, F. M. Toma, I. D. Sharp, cation-dependent light-induced halide demixing in hybrid organic–inorganic perovskites. Nano Lett. 18 (2018) 3473–3480.

[30] Z. J. Su, Y. Chen, X. G. Li, S. R. Wang, Y. Xiao, The modulation of opto-electronic properties of $CH_3NH_3PbBr_3$ crystal. J. Mater. Sci.: Mater. Electron. 28 (2017) 11053-11058.

[31] (a) Y. Yamada, T. Yamada, L. Q. Phuong, N. Maruyama, H. Nishimura, A. Wakamiya, Y. Murata, Y. Kanemitsu, Dynamic optical properties of $CH_3NH_3PbI_3$ single crystals as revealed by one- and two-photon excited photoluminescence measurements. J. Am. Chem. Soc. 137 (2015) 10456–10459; (b) W. Zhang, et al. Ultrasmooth organic–inorganic perovskite thin-film formation and crystallization for efficient planar heterojunction solar cells. Nat. Commun. 6 (2015) 6142; (c) Y. J. Fang, H. T. Wei, Q. F. Dong, J. S. Huang, Quantification of re-absorption and re-emission processes to determine photon recycling efficiency in perovskite single crystals. Nat. Commun. 8 (2017) 14417.

[32] C. Wang, X. Xu, C. Wang, F. Xie Y. Gao, Degradation of co-evaporated perovskite thin film in air, Chem. Phys. Lett. 649 (2016) 151-155.

[33] H. Xie, C. Liu, L. Lyu, D. Niu, Q. Wang, J. Huang, Y. Gao, Effects of precursor ratios and annealing on electronic structure and surface composition of $CH_3NH_3PbI_3$ perovskite films, J. Phys. Chem. C 120 (2016) 215−220.

[34] (a) S. Gonzalez-Carrero, R. E. Galian, J. Perez-Prieto, Maximizing the emissive properties of $CH_3NH_3PbBr_3$ perovskite nanoparticles, J. Mater. Chem. A 3 (2015) 9187-9193; (b) Y. Zou, Q. Meng, H. Mao D. Zhu, Substrate effect on the interfacial electronic structure of thermally-evaporated $CH_3NH_3PbI_3$ perovskite layer, Org. Electronics 41 (2017) 307.

[35] S. R. Raga, M.-C. Jung, M. V. Lee, M. R. Leyden, Y. Kato, Y. Qi, Influence of air annealing on high efficiency planar structure perovskite solar cells, Chem. Mater. 27 (2015) 1597-1603.

[36] J. Chastain, R. C. King, Handbook of X-Ray photoelectron spectroscopy, Physical Electronic Inc, New York, 1995.

[37] Y. Li, X. Xu, C. Wang, B. Ecker, J. Yang, J. Huang, Y. Gao, Light-induced degradation of $CH_3NH_3PbI_3$ hybrid perovskite thin film, J. Phys. Chem. C 121 (2017) 3904-3910.

[38] (a) W. E. Morgan, J. R. Van Wazer, Binding energy shifts in the x-ray photoelectron spectra of a series of related Group IVa compounds, J. Phys. Chem. 77 (1978) 964-969; (b) V. I. A. Nefedov, A comparison of results of an ESCA study of nonconducting solids using spectrometers of different constructions, J. Electronspectrosc. Relat. Phenom. 25 (1982) 29-47.

[39] R. Lindblad, D. Bi, B.-W. Park, J. Oscarsson, M. Gorgoi, H. Siebahn, M. Odelius, E. M. J. Johnsson, H. Rensmo, Electronic structure of $TiO_2/CH_3NH_3PbI_3$ perovskite solar cell interfaces, J. Phys. Chem. Lett. 5 (2014) 648-653.